Cell and Tissue Research (2019) 376:365–376
https://doi.org/10.1007/s00441-018-2976-x

REGULAR ARTICLE

Sialoglycoprotein isolated from *Carassius auratus* eggs promotes osteogenesis by stimulating mesenchymal stem cells to commit to osteoblast differentiation

Lei Mao[1] · Meiling Wang[1] · Xingjun Xi[2] · Yufeng Dai[1] · Na Wang[1] · Jingfeng Wang[1] · Changhu Xue[1]

Received: 1 March 2018 / Accepted: 23 November 2018 / Published online: 4 February 2019

Abstract

In this study, we explore whether the pro-osteogenic effects of sialoglycoprotein from *Carassius auratus* eggs (*Ca*-SGP) involve mesenchymal stem cells (MSCs). Ovariectomized osteoporotic mice treated with *Ca*-SGP had increased bone formation and reduced bone marrow adipose tissue. As MSCs are common progenitors of osteoblasts and adipocytes, we isolated MSCs from *Ca*-SGP-treated mice and found that they tended to differentiate into osteoblasts over adipocytes confirmed by Alizarin red and Oil red O staining. This change was seen at the gene and protein level. To further explore the effect of *Ca*-SGP on MSCs, we isolated MSCs from healthy mice and treated them with *Ca*-SGP in vitro. We discovered that *Ca*-SGP promoted MSC differentiation to osteoblasts. In addition, *Ca*-SGP promoted osteogenesis and reduced the fat in marrow cavity of adolescent mice. For the first time, our results demonstrate that *Ca*-SGP promotes osteogenesis via stimulating MSCs to commit to osteoblasts.

Keywords Sialoglycoprotein · Osteogenesis · Mesenchymal stem cell · Osteoblast · Differentiation

Introduction

Osteoporosis, a severe bone metabolic disease, affects hundreds of millions of people worldwide (Hendrickx et al. 2015). The imbalance between bone formation and bone absorption is an important inducement of osteoporosis (Min et al. 2017); however, in the past decade, there has been a growing awareness that bone remodeling is also blocked by excess fat, implying that bone and fat are both closely related to bone loss (Abdallah and Kassem 2012; Cao 2011; Kawai et al. 2009). Current therapeutic strategies for osteoporosis include inhibition of osteoclast activity and enhancement of osteoblast activity; however, the widely used drugs bisphosphonates and parathyroid hormone are costly (Brar 2010; Moro Alvarez et al. 2016), such as femoral shaft stress fractures. With a new understanding of osteoporosis pathogenesis, effective and safe treatments are to be developed.

Mesenchymal stem cells (MSCs) are multipotent cells and have been found in both bone marrow and compact bone (da Silva Meirelles et al. 2006; Pittenger et al. 1999). MSCs are common progenitors of osteoblasts and adipocytes, which are functional cells in the formation of bone and fat, respectively (Chen and Shou 2016; Nombela-Arrieta et al. 2011). Osteoblasts and adipocytes co-regulate the balance of osteogenesis and adipogenesis and have a reciprocal relationship. Therefore, as MSCs differentiate into one cell line, they gradually lose their ability to differentiate into another (Uccelli et al. 2008). Defective osteogenic differentiation of MSCs can simultaneously result in bone loss and lipoatrophy, which is supported by clinical observations that bone loss caused by age or ovariectomy is often associated with increased bone marrow fat (Cohen et al. 2012). Hence, improving the ability of MSCs to differentiate into osteoblasts is an effective therapeutic strategy to promote osteogenesis and improve osteoporosis (Matsushita and Dzau 2017; Nuttall et al. 1998).

Electronic supplementary material The online version of this article (https://doi.org/10.1007/s00441-018-2976-x) contains supplementary material, which is available to authorized users.

✉ Jingfeng Wang
jfwang@ouc.edu.cn

[1] College of Food Science and Engineering, Ocean University of China, Qingdao 266003, Shandong Province, China

[2] China National Institute of Standardization, Beijing 100191, China

Fish eggs, the main by-product of fish processing, contain all the substances necessary for hatching and various functional components, including polyunsaturated fatty acids, DHA/EPA-phospholipid, lecithin and glycoproteins (Olsen et al. 2014). However, its high-value utilization has not been explored. Sialoglycoprotein isolated from eggs of *Carassius auratus* (*Ca*-SGP) inhibits bone resorption by suppressing the activation of osteoclastogenesis (Xia et al. 2015b) and promotes osteogenesis by facilitating maturation of MC3T3-E1 pre-osteoblastic cells (Xia et al. 2015a). However, the effect of *Ca*-SGP on the modulation between bone and fat is still unknown.

Our present study is designed to explore whether the pro-osteogenic effect of *Ca*-SGP is due to effects on MSCs. We isolated MSCs from compact bone of mice and clarified this question both in vivo and in vitro. Our research establishes the basis for a novel application of *C. auratus* eggs as a functional food used to accelerate bone formation.

Materials and methods

Preparation of *Ca*-SGP

Ca-SGP was provided by Guanghua Xia (Ocean University of China, Qingdao, China) and its properties have been previously described (Xia et al. 2015a).

Animals and experimental design

Animal protocols were approved by the ethical committee of experimental animal care at Ocean University of China (certificate no. SYXK20120014). All animal experiments were carried out following institutional guidelines. Six-week-old female C57BL/6J mice (17 ± 1 g) and three-week-old male ICR mice (20 ± 2 g) were obtained from Vital River Laboratory Animal Center (Beijing, China; license ID SCXK2012-0001). Animals were housed 3–4 per cage under standard conditions (12 h light/12 h dark cycle, 23 ± 1 °C controlled temperature, food and water ad libitum).

After adaptive feeding for 1 week, C57BL/6J mice underwent bilateral ovariectomy to establish a postmenopausal osteoporosis model (OVX, $n = 24$). A sham operation group was established simultaneously (sham, $n = 8$). After 10 weeks, OVX animals were randomly divided into three groups ($n = 8$ mice per group) as follows: model (treated with physiological saline), positive control (treated with alendronate sodium; 1 mg/kg body weight) and *Ca*-SGP (treated with *Ca*-SGP; 400 mg/kg body weight). The sham-operated group was treated with physiological saline. Physiological saline or respective drugs were given by gavage once a day for 90 days (10 ml/kg body weight). After 90 days of treatment, animals were sacrificed and femurs and tibiae were quickly isolated followed by an assessment of bone mineral density, bone histomorphometry and micro-computerized tomography analysis.

After adaptive feeding for 1 week, ICR mice were randomly divided into two groups ($n = 8$ mice each): normal (treated with physiological saline) and *Ca*-SGP (treated with *Ca*-SGP; 400 mg/kg body weight). The mice were intragastrically given a volume of 10 ml/kg/bodyweight once a day for 21 days. Mice were sequentially injected with 20 mg/kw/bw tetracycline hydrochloride solution (Solarbio, Beijing, China) and 5 mg/kw/bw calcein solution (Tokyo Chemical Industry, Tokyo, Japan). The interval between the first and second injection was 10 days and the second injection was administered 2 days before sacrifice. After 21 days of treatment, animals were sacrificed to obtain femurs for subsequent experiments.

Bone mineral density and bone formation rate testing

Dual-energy X-ray absorptiometry was performed to determine the BMD of femurs using a GK99-UNIGAMMA X-RAY PLUS Bone Densitometer (L'acn, Lainate, Italy).

To analyze dynamic bone growth, proximal femurs of ICR mice were decalcified for 3 h in 10% (*w*/*v*) EDTA. After gradient dehydration using ascending grades of ethanol, samples were embedded in paraffin, sectioned (10 μm thickness) and dewaxed for 1 h. Then, anti-fluorescence quenching reagents (Solarbio, Beijing, China) were added for accurate observation under fluorescence microscopy.

Bone histomorphometry

For hematoxylin and eosin (H&E) staining, the distal femurs of C57BL/J6 mice and ICR mice were fixed in 10% (*w*/*v*) neutral formaldehyde for 24 h and decalcified in 8% (*w*/*v*) EDTA decalcifying solution for 3 weeks. Then, the decalcified samples were embedded in paraffin after dehydration with ethanol and sectioned (6 μm thickness) for subsequent staining.

Micro-computerized tomography analysis

Left tibiae were fixed with 8% neutral formaldehyde for 24 h and after washing with running water, tibiae were stored in saline. A micro-CT system (μ-CT80 scanner Scanco Medical, Bassersdorf, Switzerland) was used for μ-CT analysis and the scanning was performed at 70 kV, 114 mA. The coronal images were collected at a resolution of 10 μm per pixel and reconstructed to 3D images for morphometric analysis. Quantification of trabecular morphometric indices was performed in a defined cancellous bone area located 1 mm below the epiphyseal line of the proximal end of the tibia. Trabecular morphology was described by measuring the bone volume

fraction (bone volume/tissue volume, BV/TV), trabecular thickness (Tb.Th), trabecular number (Tb.N), trabecular separation (Tb.Sp), connectivity density (Conn.D) and structure model index (SMI).

Cell culture

The isolation of MSCs from mouse compact bone was performed as previously described (Zhu et al. 2010). MSCs were cultured in Low Glucose Dulbecco's Modified Eagle's Medium (L-DMEM; Gibco, Gaithersburg, MD) containing 15% (*v*/*v*) fetal bovine serum (FBS; Biological Industries, Kibbutz Beit-Haemeck, Israel) and 0.1% (*w*/*v*) penicillin-streptomycin (Sangon Biotech Co. Ltd., Shanghai, China) at 37 °C with 5% CO_2. Adherent MSCs were passaged with 0.25% (*w*/*v*) trypsin and 0.02% (*w*/*v*) EDTA-Na_2 (Solarbio, Beijing, China) and used for experiments at passage 3.

For immunophenotyping analysis, 1×10^6 cells were resuspended in 100 μl of cold PBS and stained with PE-conjugated anti-mouse CD44 (eBioscience, California, USA) and isotype antibodies (eBioscience, California, USA) for 30 min at 4 °C in the dark. Then, the cells were centrifuged twice at 4 °C with cold PBS (300 g, 8 min). PI (0.6 μg per million cells) was added in 300 μl cold PBS and incubated for 15 min at room temperature in the dark to evaluate the cell viability. Finally, the data were analyzed by FACSCalibur and WinMDI 2.9 software.

Cell differentiation assays

For differentiation to osteoblasts, MSCs (3×10^4/well) were seeded in a 24-well plate and induced by L-DMEM supplemented with 15% (*v*/*v*) FBS, 10^{-7} M dexamethasone (DEX; Sigma, St. Louis, MO, USA), 10 mM β-glycerol phosphate (β-GP; Sigma, St. Louis, MO, USA) and 50 μM ascorbic acid (VC; Sigma, St. Louis, MO, USA) for 21 days.

For differentiation to adipocytes, MSCs (3×10^4/well) were seeded in a 24-well plate and induced by high glucose DMEM (H-DMEM; Sigma, St. Louis, MO, USA) supplemented with 15% (*v*/*v*) FBS, 10^{-6} M DEX, 0.5 mM isobutylmethylxanthine (IBMX; 10 ng/ml; Sigma, St. Louis, MO, USA), 10 μg/ml insulin (Sigma, St. Louis, MO, USA) and 0.2 mM indomethacin (Sigma, St. Louis, MO, USA) for 8 days.

For transdifferentiation from osteoblasts to adipocytes, MSCs (3×10^4/well) were seeded in a 24-well plate and cultured with osteoplastic inducers for 21 days before switching to an adipogenic hormonal cocktail for another 14 days.

For transdifferentiation from adipocytes to osteoblasts, MSCs (3×10^4/well) were seeded in a 24-well plate and cultured with an adipogenic hormonal cocktail for 8 days before switching to osteoplastic inducers for another 28 days.

All the medium was changed every 2 days.

Alizarin red and oil red O staining

For Alizarin Red staining, media was removed and cells were washed twice with D-Hanks; then, the cells were fixed with 95% alcohol for 20 min and stained with 0.5% (*w*/*v*) Alizarin Red-Tris (Sigma, St. Louis, MO, USA) for 30 min. After washing thoroughly with deionized water, stained cells were photographed with an inverted microscope (IX51, Olympus, Tokyo, Japan).

For Oil Red O staining, cells were washed twice with D-Hanks and then fixed for 30 min with 5% (*v*/*v*) glutaraldehyde. Cells were then stained with filtered 0.5% Oil-red O (Sigma, St. Louis, MO, USA) diluted with 2/3 volume of water for 0.5 h. After washing with 60% (*v*/*v*) isopropanol, lipid droplets were photographed with an inverted microscope (IX51, Olympus, Tokyo, Japan).

Quantitative real-time polymerase chain reaction analysis

After 14 days of treatment for differentiation to osteoblasts and 8 days of treatment for differentiation to adipocytes, mRNA expression of key genes regulating osteoblast differentiation and adipocyte differentiation was examined by qRT-PCR. The primers of Runt domain-containing transcription factor 2 (Runx2), peroxisome proliferator-activated receptor-γ (PPARγ), CCAAT/enhancer binding protein-α (C/EBPα), alkaline phosphatase (ALP), osteocalcin (OCN), glucose transporter 4 (Glut4), fatty acid binding protein 4 (ap2) and beta-actin were synthesized by Sangon Biotech Co. Ltd. Total RNA was extracted using RNeasy Mini Kit (QIAGEN, Hilden, Germany) and 1 μg RNA was transcribed to cDNA with 1 μl M-MLV, 1.5 μl random primer and 2 μl dNTPs. Then, cDNA was amplified in a 25-μl reaction containing SYBR Green mix (Roche, Basel, Switzerland) using a quantitative real-time PCR thermocycler (iQ5, Bio-Rad, Hercules, CA). The amplification conditions were as follows: initial denaturation at 95 °C for 10 min followed by 40 cycles of 95 °C for 15 s, 60 °C for 10 s and 72 °C for 45 s. The relative mRNA levels were expressed as the ratio of target gene expression to the housekeeping gene β-actin. The primers used in this study are shown in Table S1.

Western blot analysis

The protein expression of PPARγ and Runx2 was measured by Western blotting. Primary rabbit anti-PPARγ (#2435) and RUNX2 (#12556) antibodies were from Cell Signaling (Beverly, MA, USA). After 14 days of treatment for differentiation to osteoblasts and 8 days of treatment for differentiation to adipocytes, cells were washed twice with ice-cold D-Hanks and lysed using RIPA buffer (Solarbio, Beijing, China) containing a protease inhibitor mixture (Solarbio, Beijing, China)

to obtain the total protein. Protein concentration was determined by BCA kit (Solarbio, Beijing, China). Equal amounts of protein were separated by SDS-PAGE and then transferred to a polyvinylidene fluoride membrane (Millipore, Bedford, MA). The membrane was blocked with 1× TBS containing 5% (*w*/*v*) BSA for 2 h at room temperature. After blocking, the membranes were incubated overnight at 4 °C with the respective primary antibodies. Subsequently, the membranes were incubated with goat-anti rabbit IgG-HRP secondary antibody (Catalog: SA00001-2, proteintech) for 2 h. Then, an ECL stain kit (Applygen, Beijing, China) and ImageJ program were used to visualize and quantify protein bands. β-actin was analyzed as a reference for total protein.

Statistical analysis

All data were presented as mean ± SD for at least three independent experiments. One-way analysis of variance (ANOVA) followed by the Tukey's test were used to assess the differences between individual groups. Differences were considered as significant with $P < 0.05$.

Results

Ca-SGP increased bone mineral density of mice with osteoporosis

BMD is regarded as an important index to evaluate bone strength and diagnose osteoporosis (Rosen 2005). As shown in Fig. 1, in the osteoporotic model group (OVX-C), femur BMD was significantly reduced by 8.83% compared with the normal group (sham). However, BMD recovered by 9.69% after 3 months of treatment with *Ca*-SGP over the OVX-C group, indicating that *Ca*-SGP promoted osteogenesis.

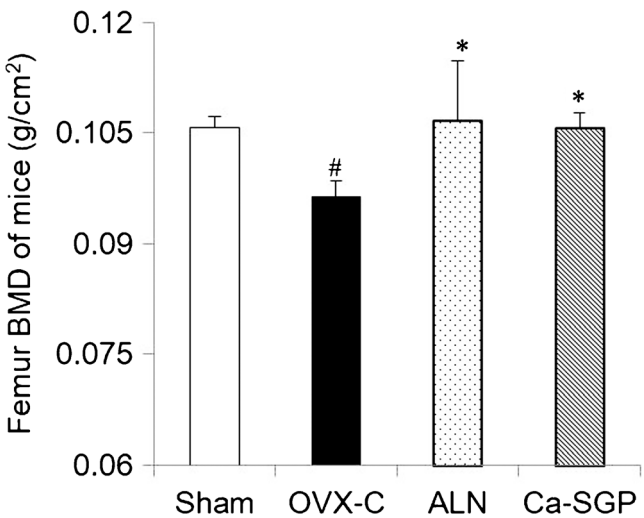

Fig. 1 *Ca*-SGP increased bone mineral density of osteoporotic mice. Femurs were collected and treated with dual-energy X-ray absorptiometry. Data are presented as the mean ± SD ($n = 8$ per group). Multiple comparisons were done using one-way ANOVA analysis. $^{\#}P < 0.05$ versus Sham group; $^{*}P < 0.05$ versus OVX-C group

Ca-SGP ameliorated cancellous bone microarchitecture

To further investigate the effects of *Ca*-SGP on bone in OVX mice, the proximal tibia was analyzed by μ-CT. The coronal images of mice proximal tibia (Fig. 2a) and 3D (Fig. 2b) images showed that *Ca*-SGP significantly prevented bone loss in OVX mice. Table 1 showed that OVX induced the deterioration of trabecular microarchitecture as evidenced by sharply decreased trabecular bone volume fraction (BV/TV), trabecular number (Tb.N), the trabecular thickness (Tb.Th) and increased trabecular separation (Tb.Sp). However, Ca-SGP rescued the damaged trabecular structure remarkably. Morphometry data indicated that compared with the OVX-C group, *Ca*-SGP increased the BV/TV, Tb.N, Tb.Th and the connectivity density (Conn.D) by 29.27%, 56.31%, 21.63% and 80.90%, respectively. Moreover, Ca-SGP decreased the Tb.Sp and structure model index (SMI) by 36.71% and 15.52%.

Ca-SGP maintained the balance of bone and fat in marrow cavities of osteoporotic mice

An increasing number of studies have found that a reciprocal relationship exists between bone quality and bone adiposity. In our study, we found that mice with ovariectomy-induced osteoporosis also had reduced trabeculae and increased bone marrow adiposity in the femoral bone marrow space. In contrast, *Ca*-SGP ameliorated these adverse changes. Histologic analysis showed that the number of trabeculae increased and bone marrow adipose tissue (BMAT) decreased in the *Ca*-SGP-treated group, indicating that *Ca*-SGP enhanced osteoblast function and weakened adipocyte function (Fig. 3).

Ca-SGP stimulated osteoporotic MSCs to differentiate into osteoblasts

Given that osteoblasts and adipocytes both originate from MSCs, we sought to determine if *Ca*-SGP influenced differentiation of MSCs. Therefore, we isolated MSCs from compact bone and cultured them in vitro. An adherent layer of typical vortex-shaped cells developed within 6 days (Fig. 4a) and flow cytometry analysis revealed that the mesenchymal surface marker CD44 was positive (Fig. 4b, c).

Then, we induced MSCs to undergo osteogenesis. Alizarin Red staining revealed that MSCs isolated from osteoporotic mice had significantly reduced osteogenic differentiation potential compared with MSCs from the normal group (Fig. 5a).

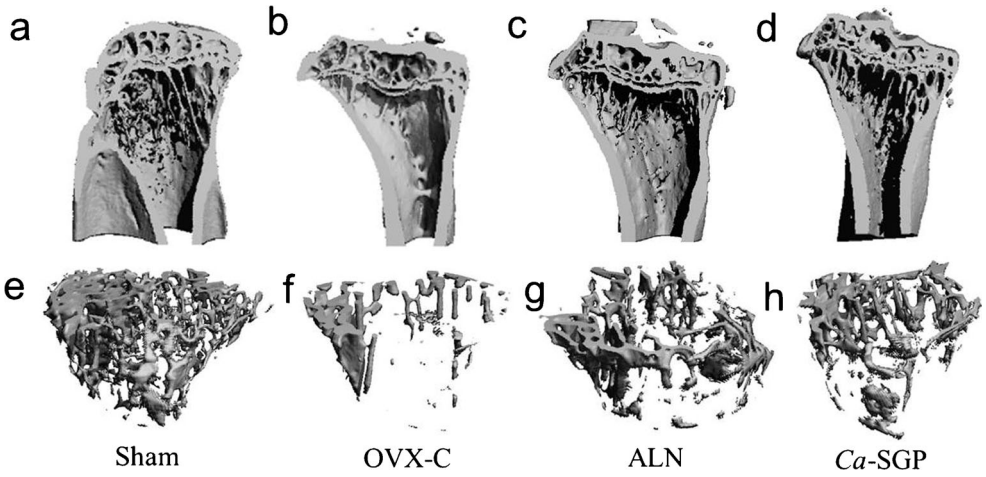

Fig. 2 Effects of *Ca*-SGP on the bone microstructure of OVX-induced osteoporotic model mice. Coronal images of the mice left proximal tibia (**a**–**d**) were scanned by μ-CT and 3D images (**e**–**h**) were reconstructed by μ-CT analysis of the area located 1 mm below the epiphyseal line of the proximal end of the tibia ($n = 5$ per group)

However, treatment with *Ca*-SGP restored differentiation potential to osteoblasts. Additionally, *Ca*-SGP up-regulated expression of osteogenic genes, such as *Runx2*, *ALP* and *OCN* and down-regulated adipogenic genes, such as *PPARγ*, *C/EBPα*, *ap2* and *Glut4* (Fig. 5b). Elevated protein expression of Runx2 and decreased protein expression of PPARγ were also observed compared to the model group in Fig. 5(c). Taken together, these data suggested that *Ca*-SGP stimulated osteoporotic MSCs to differentiate into osteoblasts.

Ca-SGP inhibited osteoporotic MSCs to differentiate into adipocytes

As the differentiate of MSCs into osteoblasts and adipocytes are opposite processes, MSCs were induced to undergo adipogenesis and Oil Red O staining was performed to determine the degree of fat droplet generation. Compared with MSCs separated from the normal group, there were more fat droplets in osteoporotic MSCs, indicating significantly enhanced adipogenic differentiation potential. As shown in Fig. 6(a,b), *Ca*-SGP decreased intracellular fat droplets in model MSCs and down-regulated expression of adipogenic genes, such as *PPARγ*, *C/EBPα*, *ap2* and *Glut4*, indicating reduced potential to differentiate into adipocytes. In addition, *Ca*-SGP up-regulated the expression of osteogenic genes, such as *Runx2*, *ALP* and *OCN*. Furthermore, decreased protein expression of PPARγ and elevated protein expression of Runx2 were also observed compared with the model group. Therefore, we concluded that *Ca*-SGP inhibited the differentiation of osteoporotic MSCs into adipocytes.

Ca-SGP improved osteogenic conversion potential and reduced adipogenic conversion potential in MSCs isolated from osteoporotic mice

As we observed that *Ca*-SGP-treated MSCs had higher expression of osteogenic markers than the model group when induced to become adipocytes (Fig. 6), we considered that higher osteogenic conversion potential remained even after 8 days of adipogenic induction. Therefore, we performed a transdifferentiation experiment from adipogenesis to

Table 1 Trabecular microstructural properties of left tibia evaluated ex vivo by micro-CT

	BV/TV	Tb.N (mm^{-1})	Tb.Th (mm)	Tb.Sp (mm)	Conn.D (mm^{-3})	SMI
Sham	6.8 ± 0.50	3.97 ± 0.21	0.070 ± 0.006	0.22 ± 0.02	85.56 ± 2.07	2.18 ± 0.11
OVX-C	4.1 ± 0.50$^{\#\#}$	1.65 ± 0.12$^{\#\#}$	0.042 ± 0.004$^{\#\#}$	0.57 ± 0.03$^{\#\#}$	17.28 ± 1.10$^{\#\#}$	2.58 ± 0.08$^{\#\#}$
ALN	6.2 ± 0.58**	2.91 ± 0.15**	0.048 ± 0.004	0.34 ± 0.02**	33.72 ± 1.62**	2.11 ± 0.07**
Ca-SGP	5.3 ± 0.47**	2.58 ± 0.11**	0.051 ± 0.004*	0.36 ± 0.03**	31.25 ± 0.86*	2.18 ± 0.06**

Data are presented as mean ± SD ($n = 5$ per group). Multiple comparisons were done using one-way ANOVA analysis followed by Tukey's test

$^{\#\#}P < 0.01$ versus sham group; $^{*}P < 0.05$; $^{**}P < 0.01$ versus OVX-C group

BV/TV bone volume fraction (bone volume/tissue volume), *Tb.N* trabecular number, *Tb.Th* trabecular thickness, *Tb.Sp* trabecular separation, *Conn.D* connectivity density, *SMI* structure model index

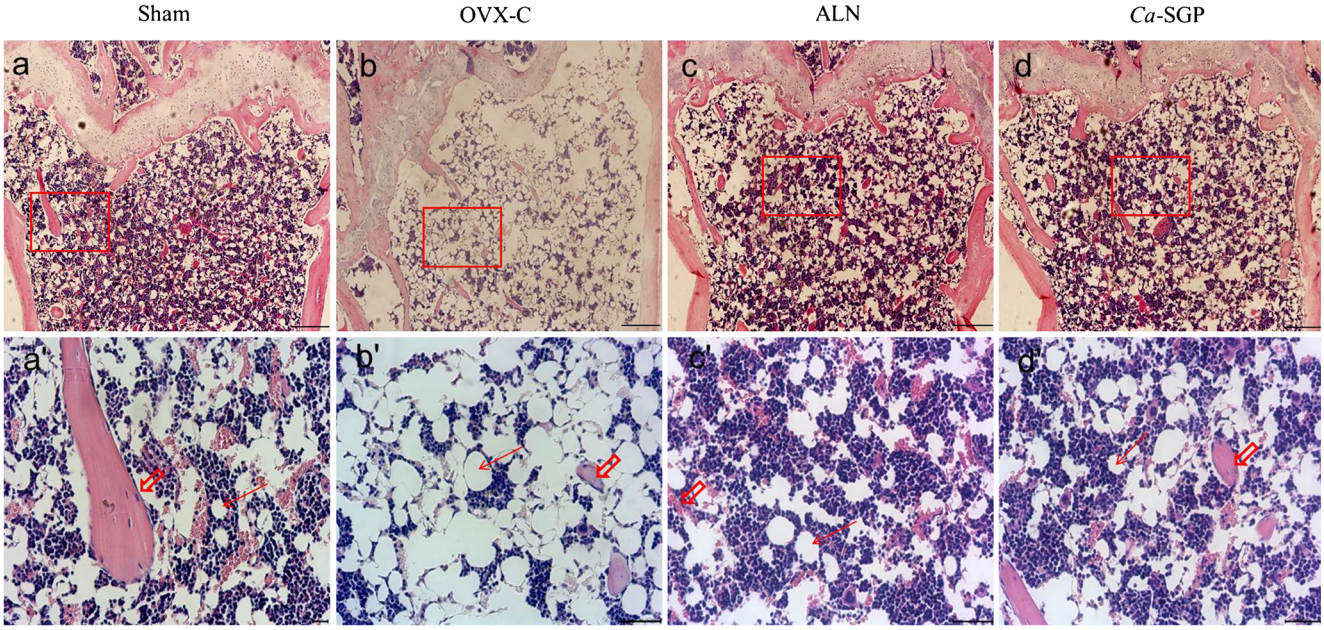

Fig. 3 *Ca*-SGP increased trabecular bone and reduced the number of adipocytes in osteoporotic mice. The distal femur was embedded in paraffin after 3 weeks of decalcification. H&E staining of 6-μm paraffin sections was performed ($n = 4$). **a'**–**d'** The regions of inserted frames in **a**–**d**, respectively. Scale bar 200 μm (**a**–**d**). Scale bar 100 μm (**a'**–**d'**). Thick arrows represent trabeculae and thin arrows represent adipocytes

osteogenesis. The results of Alizarin Red staining showed that *Ca*-SGP enhanced the potential for MSCs to undergo osteogenic conversion than cells from model mice (Fig. 7a).

Similarly, to test the hypothesis that *Ca*-SGP weakened adipogenic conversion potential during osteogenesis differentiation, we performed a transdifferentiation experiment from osteogenesis to adipogenesis. The results showed that MSCs isolated from the *Ca*-SGP group had reduced lipid droplets compared to cells from the model group (Fig. 7b), indicating that *Ca*-SGP attenuated the potential of MSCs to undergo adipogenic conversion.

Ca-SGP altered the differentiation potential of normal MSCs in vitro

To further explore whether *Ca*-SGP-induced alteration of MSC differentiation potential also exists in vitro, we isolated compact bone MSCs from normal mice and treated

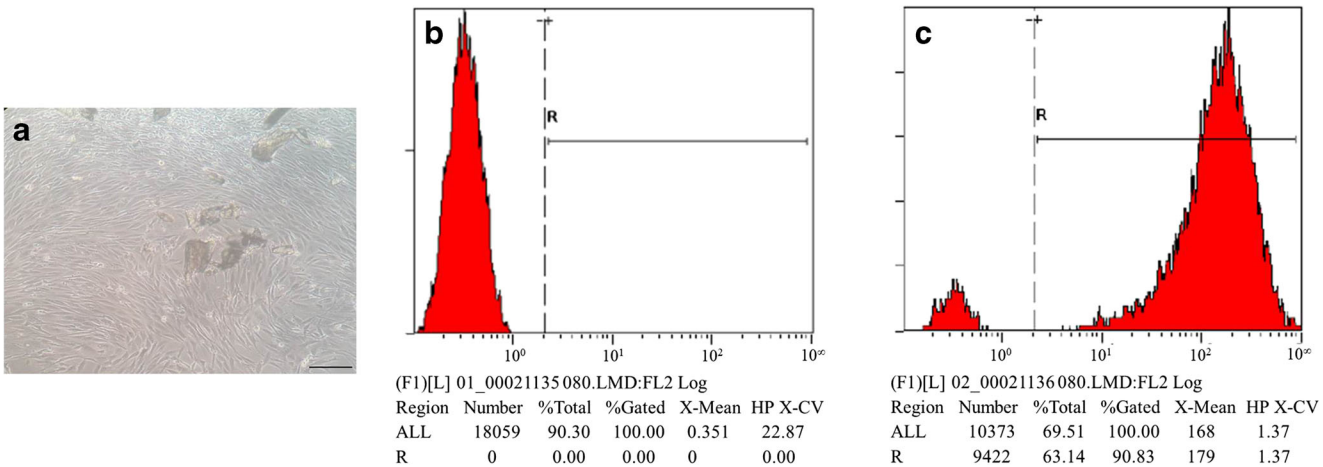

(F1)[L] 01_00021135 080.LMD:FL2 Log

Region	Number	%Total	%Gated	X-Mean	HP X-CV
ALL	18059	90.30	100.00	0.351	22.87
R	0	0.00	0.00	0	0.00

(F1)[L] 02_00021136 080.LMD:FL2 Log

Region	Number	%Total	%Gated	X-Mean	HP X-CV
ALL	10373	69.51	100.00	168	1.37
R	9422	63.14	90.83	179	1.37

Fig. 4 Morphological features and immunophenotypic characterization of compact bone-derived mouse mesenchymal stem cells. **a** An adherent layer of vortex-shaped cells developed, scale bar 100 μm. **b** The expression of the isotype control. **c** The cells were harvested by trypsin digestion and stained with phycoerythrin (PE)-conjugated anti-mouse CD44 antibody. The data were analyzed by FACSCalibur and WinMDI 2.9 software

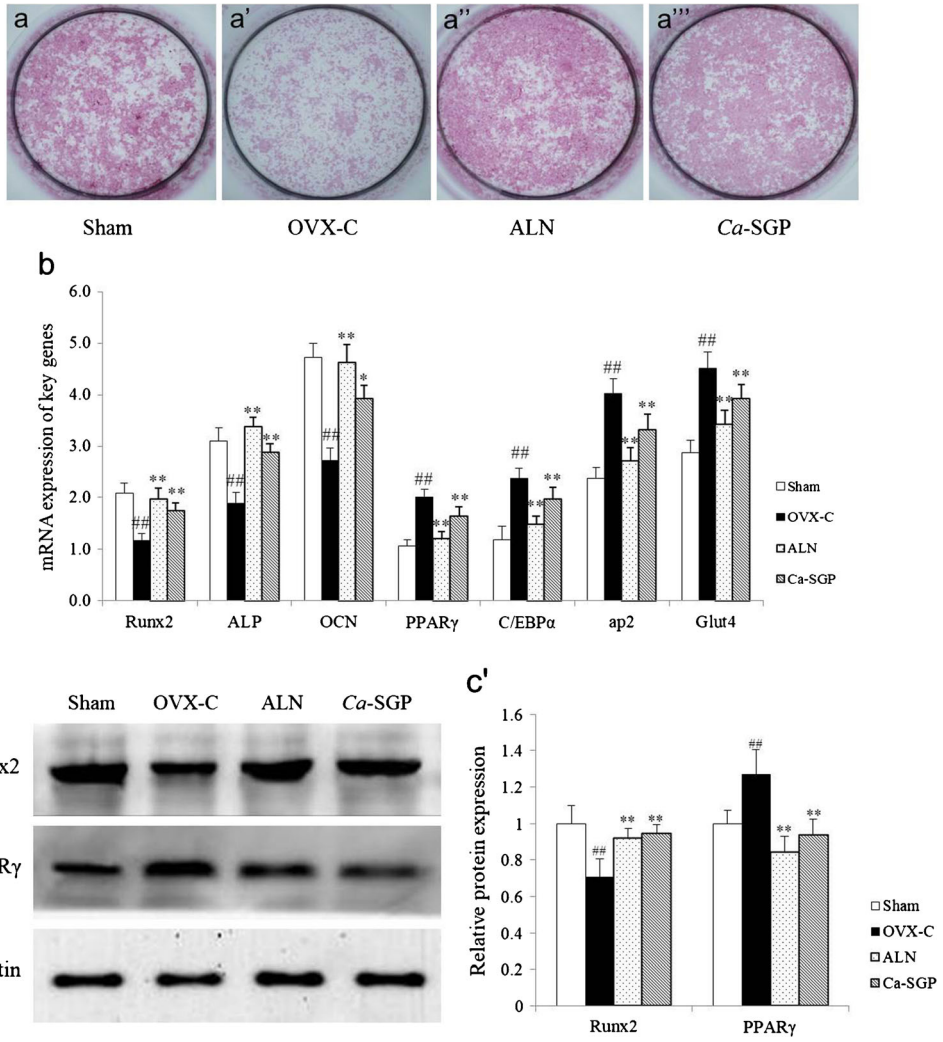

Fig. 5 *Ca*-SGP stimulated differentiation of osteoporotic MSCs into osteoblasts. **a**–**a'''** Alizarin Red staining of MSCs after inducing osteoblast differentiation for 21 days. **b** Relative expression of osteoblast and adipocyte markers in MSCs from all groups of mice after inducing osteoblast differentiation for 21 days. **c**, **c'** Protein expression and quantification of Runx2 and PPARγ in MSCs after inducing osteoblast differentiation for 14 days. Beta-actin was used as the internal control for protein test. Values are presented as mean ± SD for three independent experiments. Multiple comparisons were done using one-way ANOVA internal. $^{\#\#}P < 0.01$ versus Sham group; $^{*}P < 0.05$, $^{**}P < 0.01$ versus OVX-C group

them with *Ca*-SGP. Then, we performed the osteoblastic differentiation and adipogenic differentiation assays (Fig. 8). Results of Alizarin Red and Oil Red O staining revealed that *Ca*-SGP promoted differentiation of MSCs into osteoblasts and inhibited differentiation of MSCs into adipocytes. These in vitro results were consistent with the data observed in vivo and also verified the impact of *Ca*-SGP on MSCs.

Ca-SGP promoted osteogenesis in adolescent mice

Since *Ca*-SGP changed the differentiation potential of normal MSCs, we wondered about the influence of *Ca*-SGP in healthy mice. In 3-week-old ICR mice, BFR was performed after 21 days of gavage of *Ca*-SGP (400 mg/kg of body weight). *Ca*-SGP promoted osteogenesis as calculated by the longer distance between tetracycline hydrochloride and the calcein-labeled osteoid layers (Fig. 9).

Ca-SGP influenced the bone and fat in marrow cavity of healthy mice

We next asked whether *Ca*-SGP influenced bone and fat formation in healthy mice. As shown by histological analysis in Fig. 10, a remarkable increase of bone trabeculae and diminished adipocytes were observed in the bone marrow space.

Discussion

In the present study, our results demonstrated that *Ca*-SGP significantly increased the bone mineral density of ovariectomized mice, indicating pro-osteogenetic properties of *Ca*-SGP, consistent with previous studies (Wang et al. 2016; Xia et al. 2015a). As seen in most bone loss conditions (Rosen and Bouxsein 2006; Yao et al. 2008), we also found increased bone marrow adiposity in addition to bone loss in osteoporotic mice through histologic analysis. Treatment with *Ca*-SGP

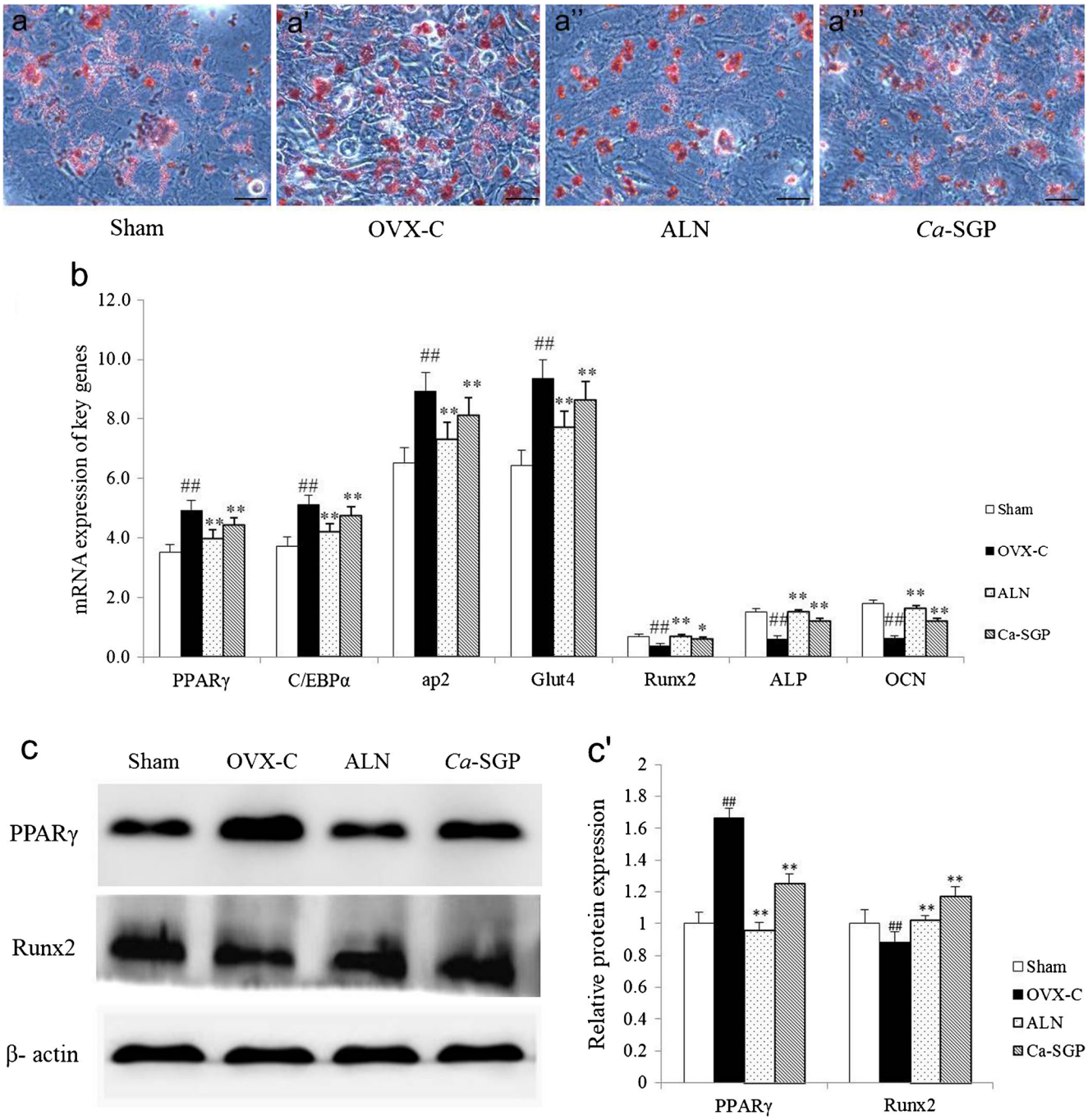

Fig. 6 *Ca*-SGP inhibited differentiation of osteoporotic MSCs into adipocytes. **a**–**a**''' Oil Red O staining of MSCs after inducing adipocyte differentiation for 8 days, scale bar 100 μm. **b** Relative expression of adipocyte and osteoblast markers in MSCs from all groups of mice after inducing adipocyte differentiation for 10 days. **c**, **c'** Protein expression and quantification of PPARγ and Runx2 in MSCs after inducing adipocyte differentiation for 8 days. Beta-actin was used as the internal control. Values are presented as mean ± SD for three independent experiments. Multiple comparisons were done using one-way ANOVA internal. ##$P < 0.01$ versus sham group; *$P < 0.05$; **$P < 0.01$ versus OVX-C group

maintained the balance of bone and fat in the marrow cavity. Due to the fact that adipocytes and osteoblasts both arise from MSCs, we next investigated whether *Ca*-SGP promoted osteogenesis by influencing MSCs.

MSCs are a type of non-hematopoietic stem cell found in the bone marrow stroma and they account for only a small fraction of nucleated cells in the bone marrow. Whole bone marrow adherent culture is a common method for isolation of MSCs in rats and humans (Goshima et al. 1991; Phinney et al. 1999). However, mouse bone marrow MSCs are not easily obtainable by this method due to contamination with hematopoietic cells. Therefore, in this mouse study, we chose an

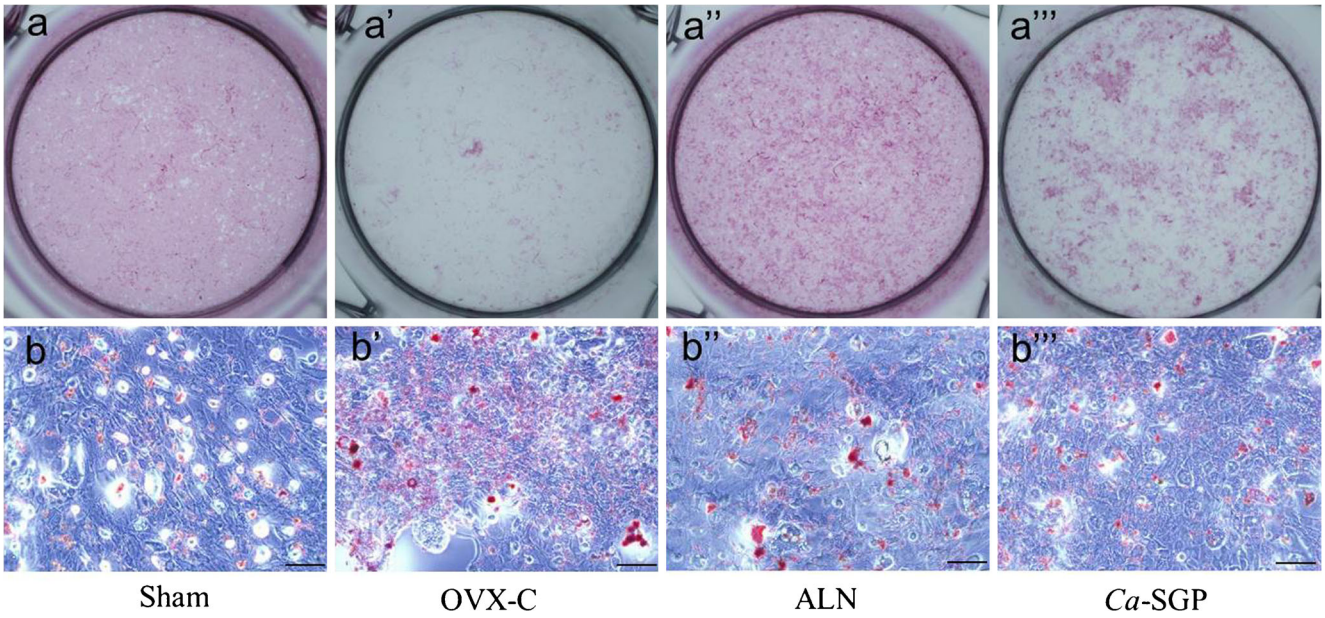

Fig. 7 *Ca*-SGP altered the transdifferentiation ability of MSCs isolated from osteoporotic mice. **a**–**a**''' Alizarin Red staining of transdifferentiated MSCs isolated from all groups of mice when induced to osteoblast differentiation. **b**–**b**''' Oil Red O staining of transdifferentiated MSCs from all groups of mice when induced to adipocyte differentiation, scale bar 100 μm

efficient and reliable protocol for the isolation of MSCs from compact bones and FACS analysis showed that these cells were positive for murine mesenchymal marker CD44, which was consistent with the literature (Tuli et al. 2003; Zhu et al. 2010), so we used these compact bone-derived MSCs for subsequent research.

A two-step process consisting of lineage commitment and maturation determines differentiation of MSCs (Chen and Shou 2016). Lineage commitment is the process by which MSCs become lineage-specific progenitors and this process is dependent on many critical signaling pathways, transcription factors and hormones (Cristancho and Lazar 2011). Runx2 is a master transcriptional regulator of differentiation of MSCs into osteoblasts (Liu et al. 2016) and PPARγ regulates differentiation of MSCs into adipocytes (Kawai and Rosen 2010). $Runx2^{+/-}$ mice have impaired skeletal mineralization (Komori et al. 1997) and repression of PPARγ by antagonists promotes MSC differentiation

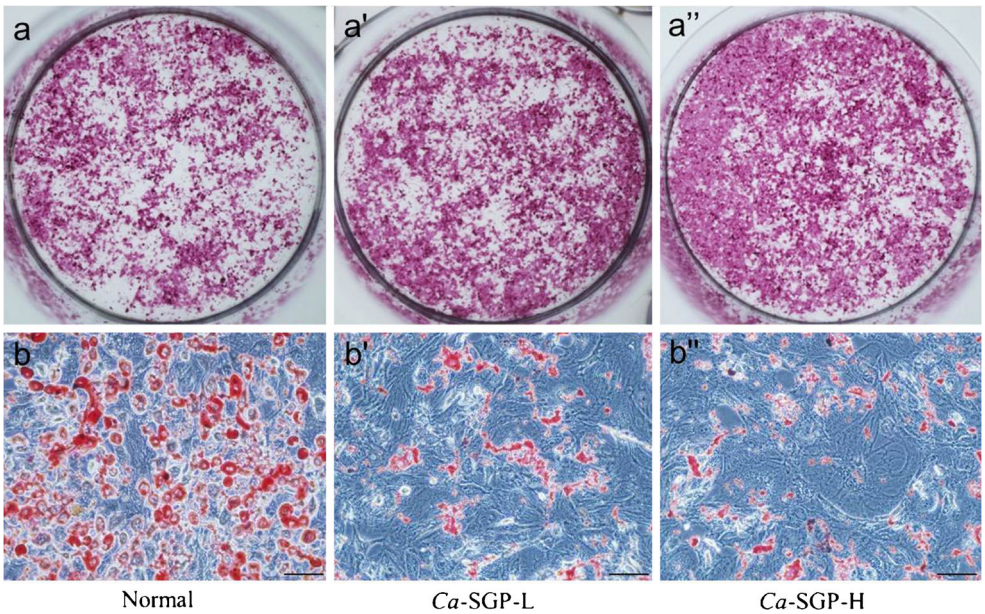

Fig. 8 *Ca*-SGP altered the differentiation potential of normal MSCs in vitro. **a**–**a**'' MSCs were treated in medium containing β-GP (10 mM) and VC (50 μg/ml) with *Ca*-SGP-L (100 μg/ml) or *Ca*-SGP-H (200 μg/ml) followed by Alizarin Red staining of MSCs. **b**–**b**'' Oil Red O staining of MSCs after inducing adipocyte differentiation for 8 days, scale bar 100 μm

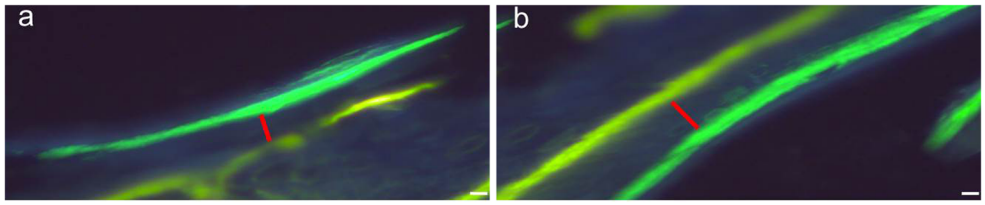

Fig. 9 *Ca*-SGP promoted osteogenesis of adolescent mice. After injection with 2.5 mg/ml tetracycline hydrochloride solution and 2.5 mg/ml calcein solution at a dose 20 mg/kg body weight, proximal femurs of ICR mice were used to analyze dynamic bone growth ($n = 3$). Scale bar 20 μm (**a**, **b**)

into osteoblasts and osteogenesis (Marciano et al. 2015). Therefore, regulation of Runx2 and PPARγ controls the MSC fate switch between osteoblasts and adipocytes and is responsible for the bone health. After lineage commitment, lineage-specific transcriptional regulators activate downstream target genes leading to a final differentiation phenotype (Chen and Shou 2016). In this study, we found a remarkable facilitative effect of *Ca*-SGP on *Runx2* expression and conversely, a suppressive effect on *PPARγ* expression. We also observed increased expression of downstream osteogenic markers such as *ALP* and *OCN* and reduced downstream adipogenic markers such as *ap2* and *Glut4*. Taken together, these results demonstrated that *Ca*-SGP has pro-osteogenic properties through acting on MSCs. This conclusion was also supported by an increase in calcium deposition and reduction in lipid formation after induction of MSCs to differentiate into osteoblasts and adipocytes.

The observed pro-osteogenic effect of *Ca*-SGP on MSCs also helped to explain our previous results. For example, the step of differentiation from preosteoblast to mature osteoblasts is included in differentiation from MSCs to mature osteoblasts; so, it is easy to understand that *Ca*-SGP promoted MC3T3-E1 differentiation. We had also previously demonstrated that *Ca*-SGP suppresses the activation of osteoclastogenesis. As the secretion of adipocytokines contributes to osteoclast formation (Cornish et al. 2006; Elefteriou et al. 2005; Takeda 2012), the reduction of adipocyte may have inhibited osteoclast function, providing new insight into understanding the effects of *Ca*-SGP on osteoclasts.

Except for differentiation to several different cell types, MSCs also have the ability to undergo transdifferentiation that reflects its plasticity. Osteoblasts differentiated from MSCs can be induced to become mature adipocytes and accordingly, mature adipocytes differentiated from MSCs have the ability to re-form the calcification matrix in an osteogenic differentiation solution (Beresford et al. 1992; Dorheim et al. 1993). In this study, we observed elevated expression of osteoblast genes, highly repressed adipocyte genes and decreased potential of adipogenic conversion in MSCs from *Ca*-SGP-treated osteoporotic mice. These observations supported that the pro-osteogenesis was due to a shift in commitment of MSCs toward osteoblasts.

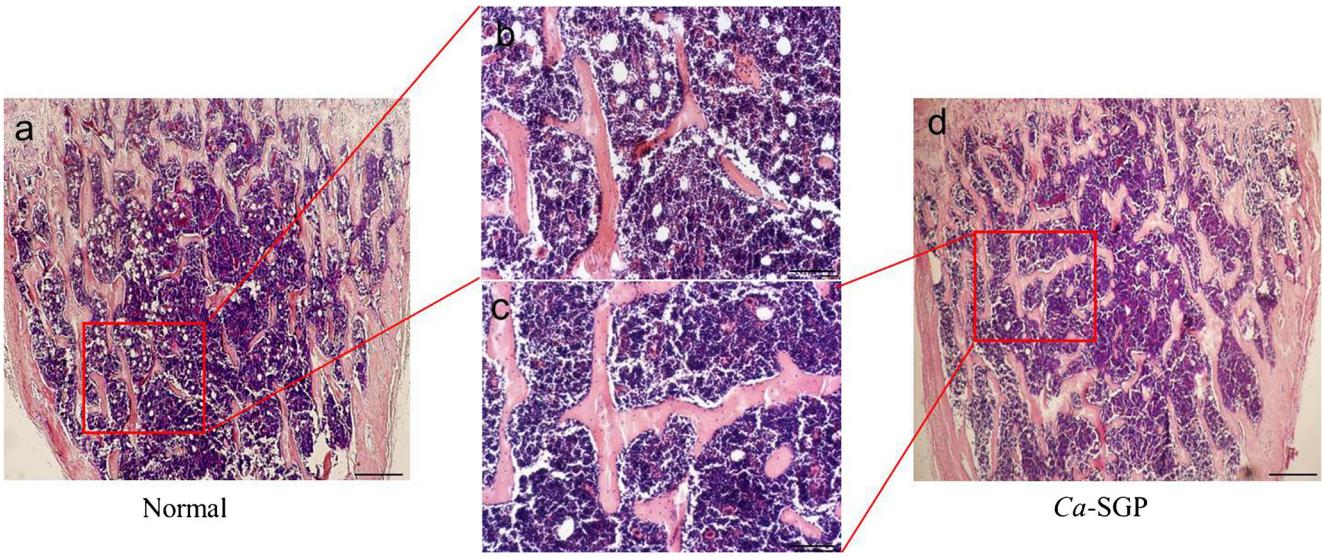

Fig. 10 *Ca*-SGP influenced the bone and fat in marrow cavity of healthy mice. The distal femur was embedded in paraffin after 3 weeks of decalcification. H&E staining of 6 μm paraffin sections was performed ($n = 3$). **b**, **c** The regions of inserted frames in **a** and **d**, respectively. Scale bar 200 μm (**a**, **d**). Scale bar 100 μm (**b**, **c**)

Conclusion

To our knowledge, our present study was the first to examine the effects of *Ca*-SGP on differentiation of MSCs. Based on the results reported here, we concluded that one of the mechanisms of *Ca*-SGP-induced osteogenesis is promoting MSCs to differentiate into osteoblasts and inhibiting its differentiation into adipocytes.

Funding information This study is financially supported by the National Key R&D Program of China (No. 2018YFC0311203), National Natural Science Foundation of China (No. 31371876), Key Research & Development Plan of Shandong Province (No. 2016YYSP017) and National Key Research and Development Program (No. 2017YFF0207800).

Compliance with ethical standards

Animal protocols were approved by the ethical committee of experimental animal care at Ocean University of China (certificate no. SYXK20120014). All animal experiments were carried out following institutional guidelines.

Conflicts of interest The authors declare that they have no competing interest.

References

Abdallah BM, Kassem M (2012) New factors controlling the balance between osteoblastogenesis and adipogenesis. Bone 50:540–545

Beresford JN, Bennett JH, Devlin C, Leboy PS, Owen ME (1992) Evidence for an inverse relationship between the differentiation of adipocytic and osteogenic cells in rat marrow stromal cell cultures. J Cell Sci 102:341–351

Brar KS (2010) Prevalent and emerging therapies for osteoporosis. Med J Armed Forces India 66:249–254

Cao JJ (2011) Effects of obesity on bone metabolism. J Orthop Surg Res 6:30

Chen Q, Shou P (2016) Fate decision of mesenchymal stem cells: adipocytes or osteoblasts? Cell Death Differ 23:1128–1139

Cohen A, Dempster DW, Stein EM, Nickolas TL, Zhou H, McMahon DJ, Muller R, Kohler T, Zwahlen A, Lappe JM, Young P, Recker RR, Shane E (2012) Increased marrow adiposity in premenopausal women with idiopathic osteoporosis. J Clin Endocrinol Metab 97: 2782–2791

Cornish J, Callon KE, Watson M, Lin J, Reid IR (2006) Resistin, an adipocytokine, stimulates osteoblast and osteoclast proliferation. Bone 38:9

Cristancho AG, Lazar MA (2011) Forming functional fat: a growing understanding of adipocyte differentiation. Nat Rev Mol Cell Biol 12:722–734

Dorheim MA, Sullivan M, Dandapani V, Wu X, Hudson J, Segarini PR, Rosen DM, Aulthouse AL, Gimble JM (1993) Osteoblastic gene expression during adipogenesis in hematopoietic supporting murine bone marrow stromal cells. J Cell Physiol 154:317–328

Elefteriou F, Ahn JD, Takeda S, Starbuck M, Yang X, Liu X, Kondo H, Richards WG, Bannon TW, Noda M (2005) Leptin regulation of bone resorption by the sympathetic nervous system and CART. Nature 434:514–520

Goshima J, Goldberg VM, Caplan AI (1991) The osteogenic potential of culture-expanded rat marrow mesenchymal cells assayed in vivo in calcium phosphate ceramic blocks. Clin Orthop Relat Res 262:298–311

Hendrickx G, Boudin E, Van Hul W (2015) A look behind the scenes: the risk and pathogenesis of primary osteoporosis. Nat Rev Rheumatol 11:462–474

Kawai M, Rosen CJ (2010) PPARgamma: a circadian transcription factor in adipogenesis and osteogenesis. Nat Rev Endocrinol 6:629–636

Kawai M, Devlin MJ, Rosen CJ (2009) Fat targets for skeletal health. Nat Rev Rheumatol 5:365–372

Komori T, Yagi H, Nomura S, Yamaguchi A, Sasaki K, Deguchi K, Shimizu Y, Bronson RT, Gao YH, Inada M, Sato M, Okamoto R, Kitamura Y, Yoshiki S, Kishimoto T (1997) Targeted disruption of Cbfa1 results in a complete lack of bone formation owing to maturational arrest of osteoblasts. Cell 89:755–764

Liu Z, Yao X, Yan G, Xu Y, Yan J, Zou W, Wang G (2016) Mediator MED23 cooperates with RUNX2 to drive osteoblast differentiation and bone development. Nat Commun 7:11149

Marciano DP, Kuruvilla DS, Boregowda SV, Asteian A, Hughes TS, Garcia-Ordonez R, Corzo CA, Khan TM, Novick SJ, Park H, Kojetin DJ, Phinney DG, Bruning JB, Kamenecka TM, Griffin PR (2015) Pharmacological repression of PPARgamma promotes osteogenesis. Nat Commun 6:7443

Matsushita K, Dzau VJ (2017) Mesenchymal stem cells in obesity: insights for translational applications. Lab Invest 97:1158–1166

Min SK, Kang HK, Jung SY, Jang DH, Min BM (2017) A vitronectin-derived peptide reverses ovariectomy-induced bone loss via regulation of osteoblast and osteoclast differentiation. Cell Death Differ 25:268–281

Moro Alvarez MJ, Neyro JL, Castaneda S (2016) Therapeutic holidays in osteoporosis: long-term strategy of treatment with bisphosphonates. Med Clin 146:24–29

Nombela-Arrieta C, Ritz J, Silberstein LE (2011) The elusive nature and function of mesenchymal stem cells. Nat Rev Mol Cell Biol 12:126–131

Nuttall ME, Patton AJ, Olivera DL, Nadeau DP, Gowen M (1998) Human trabecular bone cells are able to express both osteoblastic and adipocytic phenotype: implications for osteopenic disorders. J Bone Min Res 13:371–382

Olsen RL, Toppe J, Karunasagar I (2014) Challenges and realistic opportunities in the use of by-products from processing of fish and shellfish. Trends Food Sci Technol 36:144–151

Phinney DG, Kopen G, Isaacson RL, Prockop DJ (1999) Plastic adherent stromal cells from the bone marrow of commonly used strains of inbred mice: variations in yield, growth, and differentiation. J Cell Biochem 72:570–585

Pittenger MF, Mackay AM, Beck SC, Jaiswal RK, Douglas R, Mosca JD, Moorman MA, Simonetti DW, Craig S, Marshak DR (1999) Multilineage potential of adult human mesenchymal stem cells. Science (New York, NY) 284:143–147

Rosen CJ (2005) Postmenopausal Osteoporosis. N Engl J Med 353:595–603

Rosen CJ, Bouxsein ML (2006) Mechanisms of disease: is osteoporosis the obesity of bone? Nat Clin Pract Rheumatol 2:35–41

da Silva Meirelles L, Chagastelles PC, Nardi NB (2006) Mesenchymal stem cells reside in virtually all post-natal organs and tissues. J Cell Sci 119:2204–2213

Takeda S (2012) Leptin and bone signaling. Endocrine 29:1–10

Tuli R, Seghatoleslami MR, Tuli S, Wang ML, Hozack WJ, Manner PA, Danielson KG, Tuan RS (2003) A simple, high-yield method for obtaining multipotential mesenchymal progenitor cells from trabecular bone. Mol Biotechnol 23:37–49

Uccelli A, Moretta L, Pistoia V (2008) Mesenchymal stem cells in health and disease. Nat Rev Immunol 8:726–736

Wang F, Wang Y, Zhao Y, Zhan Q, Yu P, Wang J, Xue C (2016) Sialoglycoprotein isolated from eggs of Carassius auratus ameliorates osteoporosis: an effect associated with regulation of the Wnt/β-catenin pathway in rodents. J Agric Food Chem 64:2875–2882

Xia G, Wang S, He M, Zhou X, Zhao Y, Wang J, Xue C (2015a) Anti-osteoporotic activity of sialoglycoproteins isolated from the eggs of Carassius auratus by promoting osteogenesis and increasing OPG/RANKL ratio. J Funct Foods 15:137–150

Xia G, Yu Z, Zhao Y, Wang Y, Wang S, He M, Wang J, Xue C (2015b) Sialoglycoproteins isolated from the eggs of Carassius auratus prevents osteoporosis by suppressing the activation of osteoclastogenesis related NF-κB and MAPK pathways. J Funct Foods 17:491–503

Yao W, Cheng Z, Busse C, Pham A, Nakamura MC, Lane NE (2008) Glucocorticoid excess in mice results in early activation of osteoclastogenesis and adipogenesis and prolonged suppression of osteogenesis: a longitudinal study of gene expression in bone tissue from glucocorticoid-treated mice. Arthr Rheum 58:1674–1686

Zhu H, Guo Z-K, Jiang X-X, Li H, Wang X-Y, Yao H-Y, Zhang Y, Mao N (2010) A protocol for isolation and culture of mesenchymal stem cells from mouse compact bone. Nat Protoc 5:550–560